Catal Lett (2008) 124:405–412
DOI 10.1007/s10562-008-9493-6

Comparative Study on Catalytic Performances for Low-temperature CO Oxidation of Cu–Ce–O and Cu–Co–Ce–O Catalysts

Yan Su · Shuping Wang · Tongying Zhang · Shurong Wang · Baolin Zhu · Jianliang Cao · Zhongyong Yuan · Shoumin Zhang · Weiping Huang · Shihua Wu

Received: 23 January 2008 / Accepted: 11 April 2008 / Published online: 30 April 2008

Abstract Two series of Cu–Ce–O and Cu–Co–Ce–O catalysts were prepared by co-precipitation method. The prepared catalysts were characterized by XRD, IR, TPR, XPS, BET and ICP-AES. The catalytic activities of the catalysts for low-temperature CO oxidation were evaluated through a microreactor-GC system. TPR results indicate that the addition of cobalt to the Cu–Ce–O can increase the dispersion of copper oxide, and the interaction between cobalt and copper can enhance the reducibility of each other. XPS analysis show that Ce^{4+}, Cu^{2+}, along with Co_3O_4, are present on the surface of $Cu_{0.4}Co_{0.6}Ce_4$ catalyst. The Co/Cu atomic ratio and the calcination temperature have significant effect on the activities of the catalysts. Compared with Cu_1Ce_4 catalyst, the $Cu_{0.4}Co_{0.6}Ce_4$ catalyst has better activity and thermal stability.

Keywords Comparative study · Cu–Ce–O · Cu–Co–Ce–O · Low-temperature CO oxidation

1 Introduction

Carbon monoxide, known as the main air pollutant, is predominately emitted from the exhaust of motor vehicles and the combustion of fossil fuels. CO can be photochemically oxidized to CO_2 by consuming ozone or/and its transients in the atmosphere, which will break ozone regeneration and affect the ozone layer that protects living organisms on the earth from intense ultraviolet ray's radiation. Hence, the elimination of CO at low-temperature is very important in the environment pollution control.

In recent years, ceria has attracted much attention because of its high capacity to store and release oxygen and well-known low temperature reducibility, making more oxygen available for the oxidation process [1–3]. Catalysts based on ceria present a broad application, such as three-way catalysts for automobile exhaust gas emission control, removal of trace CO in the enclosed atmospheres, gas sensors, electrocatalysts over fuel cell electrodes [2, 3]. Doping of ceria by divalent or trivalent ions can increase the concentration of oxygen vacancies or improve its thermal stability [4]. The main effect of doping is to activate the oxygen atoms on the surface of the oxide and to facilitate the formation of an oxygen vacancy during CO oxidation [5]. Tremendous efforts have been devoted to improve the activity, selectivity and stability of CeO_2-based catalyst by doping CuO, Fe_2O_3, Co_3O_4 [1–3, 6–8]. Recently, CuO/CeO_2 catalyst has shown promising properties for CO oxidation [9]. Tada et al. [10] prepared Cu^{1+}-clusters on CeO_2 support, which were found to be highly active and selective for preferential oxidation (PROX) of CO in excess H_2 with H_2O and CO_2 under practical fuel-cell operating conditions. In our earlier work, many works were carried out to study the CuO/CeO_2 catalyst for low temperature CO oxidation [2, 11, 12]. In addition, it was found that the addition of ZrO_2 can improve the stability of CuO/CeO_2-based catalyst [13]. Sirichaiprasert et al. [14] reported that Fe_2O_3 could promote the active species of Cu–Ce–Fe–O catalysts to obtain catalytic activities. Chen et al. [15] found that incorporating Sn^{4+} into CeO_2 not only increased the mobility of lattice oxygen but also promoted the activity of the selective CO oxidation.

It is reported that Co_3O_4 is excellent low-temperature oxidation catalyst, which can oxidize CO even at room

Y. Su · S. Wang · T. Zhang · S. Wang · B. Zhu · J. Cao · Z. Yuan · S. Zhang · W. Huang · S. Wu (✉)
Department of Chemistry, Nankai University, Tianjin 300071, China
e-mail: wushh@nankai.edu.cn

temperature [16, 17]. The high activity of Co_3O_4 is mainly because the Co–O bond strength of Co_3O_4 is relatively weak and leads to desorption of more lattice oxygen [1, 18]. It has been found that the addition of cobalt can improve CO oxidation activities of Pt/SiO_2 and Au/SiO_2 catalysts [19, 20]. Additionally, Co_3O_4 also has excellent thermal stability [21]. Because of this, it seems reasonable to develop a Ceria-based catalyst doped with copper and cobalt, which would have either high activity for low-temperature CO oxidation or high thermal stability.

In this paper, the Cu–Ce–O and Cu–Co–Ce–O catalysts were studied. The catalysts were synthesized by co-precipitation and characterized by means of XRD, IR, H_2-TPR, XPS, BET and ICP-AES. The effects of different Co/Cu atomic ratio and calcination temperature on the catalytic activity were investigated in detail.

2 Experimental

2.1 Catalyst Preparation

The catalysts containing copper, cobalt and cerium (abbreviated as $Cu_xCo_yCe_z$ and x, y, z are denoted as the atomic ratio of the metals) were synthesized by co-precipitation method. The calculated amounts of copper nitrate trihydrate ($Cu(NO_3)_2 \cdot 3H_2O$), cerium nitrate hexahydrate ($Cec(NO_3)_3 \cdot 6H_2O$) and cobalt acetate tetrahydrate ($Co(Ac)_2 \cdot 4H_2O$) were dissolved in distilled water, then stirred about 20 min and a homogeneous solution was obtained. A sodium carbonate solution (0.25 mol L^{-1}) was dropped slowly into the above mixed aqueous solution under vigorous stirring until the pH value of mixed solution was 8–9. The resulting precipitate was aged for 3 h and then washed with distilled water several times for removing unwanted ions. The precursors were dried at 80 °C for 20 h and calcined at 550 °C in air for 5 h in a muffle furnace. The Cu–Ce–O catalysts with different Cu/Ce atomic ratio (abbreviated as Cu_xCe_y), Co–Ce–O (abbreviated as Co_xCe_y), CuO, CeO_2 and Co_3O_4 were also prepared by the same method. In order to investigate the effect of the calcination temperature on the catalytic activities of the catalysts, the catalysts were calcined at different temperatures in air for 5 h.

2.2 Catalyst Characterization

The X-ray diffraction patterns were recorded by using a D/MAX-2500 diffractometer with Cu Kα radiation at 40 kV and 100 mA. The data were collected in the 2θ range of 10–80° with a scan rate of 8°/min. The diffraction peaks of the crystalline phase were compared with those of standard compounds reported in the JCPDS Date File. The mean particle sizes were estimated by using Scherrer's equation.

The infrared spectra (IR) were recorded with a model MAGNA-560 Infrared Fourier Transform Spectrometer (Nicolet) in the range of 4,000–400 cm^{-1} with a resolution of 4 cm^{-1}. One milligram of each powder sample was diluted with 100 mg of potassium bromide (KBr) powder.

Temperature-programmed reduction (TPR) experiments were employed to investigate the reducibility of the samples and performed on a TPDRO 1100 apparatus supplied by Thermo-Finnigan Company. About 20 mg of the sample was reduced in a flow rate of 20 mL min^{-1} of 5% H_2 in N_2 at a heating rate of 10 °C min^{-1} from room temperature to 1,000 °C. The hydrogen consumption during the reduction was monitored continuously by a thermal conductivity detector (TCD).

X-ray photoelectron spectra were performed with a Kratos Axis Ultra DLD spectrometer employing a monochromated Al-Kα X-ray source (hν = 1,486.6 eV), hybrid (magnetic/electrostatic) optics, multi-channel plate and delay line detector (DLD). All binding energies were referenced to the adventitious C 1 s line at 284.6 eV (1 eV = 1.602×10^{-19} J).

Nitrogen adsorption–desorption isotherms at −196 °C were collected using a Quantachrome NOVA 2000e sorption analyzer. The specific surface area (S_{BET}) was calculated following the multi-point BET (Brunauer-Emmett-Teller) procedure.

The amounts of Cu, Co and Ce in the catalyst were determined by inductively coupled plasma/atomic emission spectrometry (ICP-AES) (IRIS-ADVATAGE).

2.3 Catalytic Activity Tests

The activities of the catalysts were evaluated in a continuous fixed-bed flow micro-reactor under atmospheric pressure, using 200 mg catalyst powder. A stainless steel tube with an inner diameter of 8 mm was chosen as the reactor tube. The reaction gas mixture was passed through the reactor tube with the air flow rate of 33 mL/min and the CO gas flow rate of 3.3 mL/min. A typical weight hourly space velocity (F/W) was 11,000 mL $h^{-1}g^{-1}$. The reactant and product compositions were analyzed on-line by a GC-900A gas chromatograph equipped with a thermal conductivity detector (TCD). The activity was expressed by the conversion of CO.

3 Results and Discussion

3.1 Characterization of Catalysts

Figure 1 shows the XRD patterns of Cu–Co–Ce–O catalysts with varying Co/Cu atomic ratios calcined at 550 °C. For comparison, the Cu_1Ce_4 and Co_1Ce_4 catalysts are also

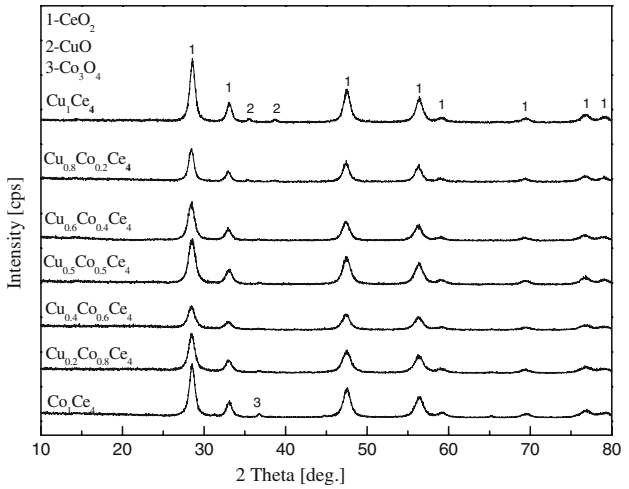

Fig. 1 XRD patterns of Cu_1Ce_4, Co_1Ce_4 and $Cu_xCo_{1-x}Ce_4$ catalysts calcined at 550 °C

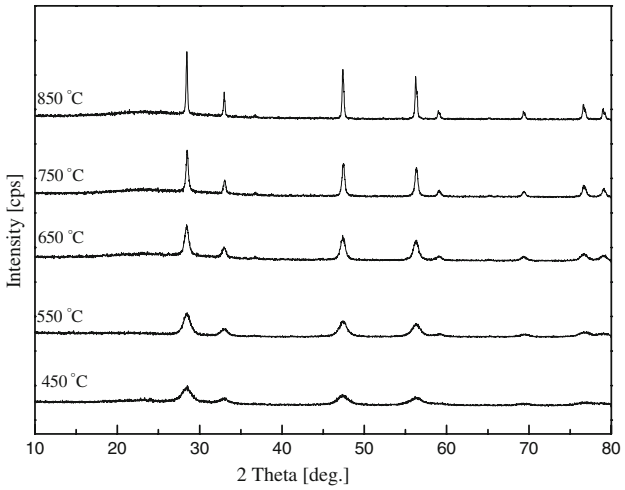

Fig. 2 XRD patterns of $Cu_{0.4}Co_{0.6}Ce_4$ catalysts calcined at different temperatures

included in the same figure. Diffractions presenting the cubic, fluorite type of CeO_2 (compared with JCPDS Date File # 34-394) are clearly observed for all the catalysts. It is also noticed that no obvious CuO diffraction can be detected when the Co/Cu atomic ratio is above 1/4 in the catalysts. This result may be due to the fine dispersion of CuO species or the formation of a solid solution or a combination of the above two states [2]. When the Co/Cu atomic ratio is below 2/3, two small peaks attributed to CuO phase can be observed at 35.4 and 38.8° of 2θ, demonstrating the formation of bulk CuO. There is no reflection characteristic of Co_3O_4 structure in the spectra of the catalysts when the Co/Cu atomic ratio is below 4/1, demonstrating that Co_3O_4 is highly dispersed or exists as amorphous surface species in the catalysts [22]. However, when the Co/Cu atomic ratio approaches to 4/1, a small peak of Co_3O_4 is detected at 36.8°.

Figures 2 and 3 present the XRD patterns of $Cu_{0.4}Co_{0.6}Ce_4$ and Cu_1Ce_4 catalysts calcined at different temperatures for 5 h, respectively. It can be seen that the peak intensities of the two series of catalysts increase with the increase of the calcination temperature. No reflection of Co_3O_4 is observed in Fig. 2 for the $Cu_{0.4}Co_{0.6}Ce_4$ catalysts calcined at 450 and 550 °C. When the temperature is higher than 550 °C, a small peak assigned to Co_3O_4 appears. It should be attributed to the aggregation of Co_3O_4 particles. However, XRD peaks due to CuO are not detected in the $Cu_{0.4}Co_{0.6}Ce_4$ catalysts calcined at different temperatures. From Fig. 3, it can be noticed that two small peaks corresponding to CuO phase are observed for the Cu_1Ce_4 catalysts calcined at different temperatures.

The mean CeO_2 and CuO particle sizes evaluated from line broadening of CeO_2 (111) and CuO (111) diffraction peaks by means of Scherrer's equation are summarized in Table 1. It can be clearly seen that the calcination

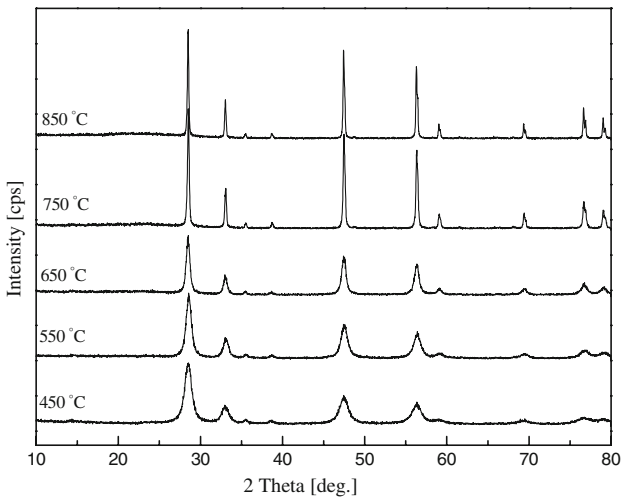

Fig. 3 XRD patterns of Cu_1Ce_4 catalysts calcined at different temperatures

temperature has a great influence on the particle sizes of CeO_2 and CuO. The increase of the calcination temperature leads to the agglomeration of the particles, and therefore to an increase of the particle size. It is interesting, when the calcination temperature rise to 850 °C, the particle size of CeO_2 in $Cu_{0.4}Co_{0.6}Ce_4$ catalyst (62.3 nm) is much smaller than that in Cu_1Ce_4 catalyst (164.5 nm), indicating that the addition of cobalt to Cu–Ce–O catalyst can enhance the thermal stability of the catalyst.

Figure 4 shows the IR spectra of Co_1Ce_4 and $Cu_{0.4}Co_{0.6}Ce_4$. Co_1Ce_4 shows two obvious bands at about 663 cm^{-1} (v_1)and 568 cm^{-1} (v_2), which can be attributed to the stretching vibration of Co–O bond. It confirms that the cobalt species exists as Co_3O_4. This is consistent with XRD result where Co_3O_4 is the only detected Co-containing phase. The v_1 band is attributed to OB_3

Table 1 The particle sizes, surface areas and catalytic activities for low temperature CO oxidation of Cu_xCe_4, Co_1Ce_4 and $Cu_xCo_{1-x}Ce_4$ catalysts

Catalysts	Calcination temperature (°C)	Particle size (nm)		Surface area (m^2/g)	CO conversion ($T_{100\%}$/°C)
		CeO_2	CuO		
$Cu_{0.7}Ce_4$	550	–	–	–	120 °C
$Cu_{1.5}Ce_4$	550	–	–	–	95 °C
Cu_1Ce_4	550	11.8	13.9	48.5	92 °C
$Cu_{0.8}Co_{0.2}Ce_4$	550	11.5	–	–	115 °C
$Cu_{0.6}Co_{0.4}Ce_4$	550	9.1	–	–	95 °C
$Cu_{0.5}Co_{0.5}Ce_4$	550	9.2	–	–	85 °C
$Cu_{0.4}Co_{0.6}Ce_4$	550	9.1	–	69.6	75 °C
$Cu_{0.2}Co_{0.8}Ce_4$	550	10.1	–	–	85 °C
Co_1Cu_4	550	10.2	–	42.4	145 °C
Cu_1Ce_4	450	8.2	10.6	–	98 °C
Cu_1Ce_4	650	13.3	16.0	–	105 °C
Cu_1Ce_4	750	38.8	25.9	–	115 °C
Cu_1Ce_4	850	164.5	39.5	–	180 °C
$Cu_{0.4}Co_{0.6}Ce_4$	450	5.6	–	–	75 °C
$Cu_{0.4}Co_{0.6}Ce_4$	650	11.5	–	–	100 °C
$Cu_{0.4}Co_{0.6}Ce_4$	750	25.5	–	–	110 °C
$Cu_{0.4}Co_{0.6}Ce_4$	850	62.3	–	–	127 °C
CuO	550	–	–	–	200 °C
Co_3O_4	550	–	–	–	130 °C
CeO_2	550	–	–	–	250 °C ($T_{25\%}$)

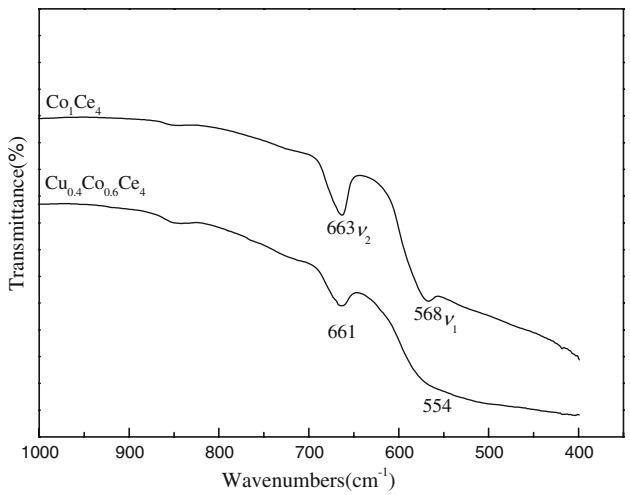

Fig. 4 IR spectra of Co_1Ce_4 and $Cu_{0.4}Co_{0.6}Ce_4$ catalysts calcined at 550 °C

vibration in the spinel lattice, where B denotes the Co^{3+} in octahedral hole, while the ν_2 is characteristic of ABO_3 vibration in the spinel lattice, where A denotes the Co^{2+} in tetrahedral hole [23–25]. Comparing ν_1 and ν_2 bands of Co_1Ce_4 with those of $Cu_{0.4}Co_{0.6}Ce_4$, it can be seen that the two bands in $Cu_{0.4}Co_{0.6}Ce_4$ shift slightly to a lower wavenumber. It is likely due to the higher surface area of the catalyst (compared with Cu_1Ce_4 and Co_1Ce_4, shown in Table 1) or that the synergetic interaction among copper, cobalt and ceria species in the catalyst can weaken the Co–O bond strength. The redistribution of free electrons between the surface and the bulk results in a decrease of the bond force constant, and consequently the bands shift to red [25].

The H_2-TPR profiles of $Cu_{0.4}Co_{0.6}Ce_4$, Cu_1Ce_4 and Co_1Ce_4 catalysts calcined at 550 °C are shown in Fig. 5. The peaks at about 800 °C in the three profiles are attributed to the reduction of bulk oxygen atoms in CeO_2 [26]. The Cu_1Ce_4 catalyst shows four reduction peaks at about 176, 219, 234 and 287 °C, namely α_1, β_1, γ_1 and δ_1, respectively. Avgouropoulos and Ioannides [27] reported that there were three overlapping reduction peaks presented in the CuO–CeO_2 catalyst: a low-intensity, low-temperature peak at 168 °C represented the reduction of copper ions strongly interacting with CeO_2 and two peaks of higher intensity at 210 and 255 °C were attributed to the reduction of larger CuO particles less associated with ceria. Liu and Flytzani-Stephanopoulos [28] reported two reduction peaks, where the reduction of copper oxide clusters strongly interacting with ceria were observed in the range of 125–175 °C, while larger CuO particles, non-associated with CeO_2, were reduced at ~200 °C. Our group [2] preciously reported that

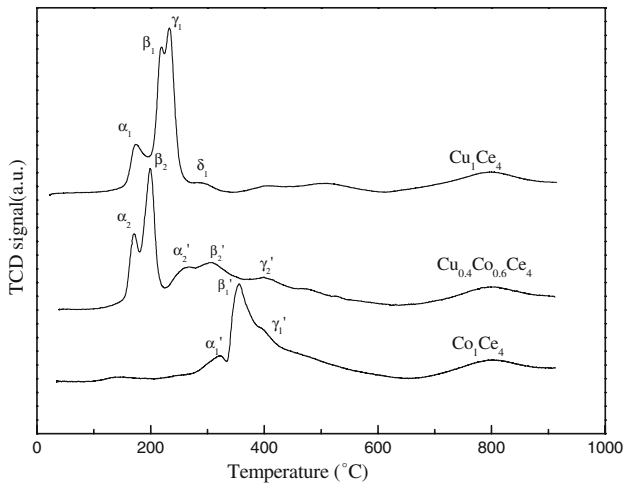

Fig. 5 H_2-TPR profiles of Cu_1Ce_4, Co_1Ce_4 and $Cu_{0.4}Co_{0.6}Ce_4$ catalysts calcined at 550 °C

there were four overlapping reduction peaks presented in CuO–CeO_2 catalyst: the peaks in the range of 134–140 °C and 183–204 °C were attributed to the reduction of non-crystalline CuO strongly interacting with CeO_2 and the reduction of larger CuO particles less associated with CeO_2, respectively. The peaks in the range of 215–219 °C and 248 °C represented the reduction of bulk copper oxide associated with CeO_2 to some extent and the reduction of pure bulk copper oxide, respectively. In the case of our study, the peak α_1 at 176 °C is ascribed to the reduction of copper ions strongly interacting with CeO_2. The peaks β_1 at 219 °C and γ_1 at 234 °C are due to the reduction of larger CuO particles (smaller than pure bulk CuO particles) less associated with CeO_2. The peak δ_1 at 287 °C represent the reduction of pure bulk CuO. Co_1Ce_4 catalyst has mainly two reduction peaks at about 322 and 356 °C with a shoulder peak at 400 °C, namely α_1', β_1' and γ_1'. Vob et al. [29] reported three reduction peaks for pure Co_3O_4: the peak at 272 °C was attributed to the reduction of Co^{3+} to Co^{2+}, the main signal at 377 °C and the shoulder one at 430 °C represented the reduction of CoO to metallic Co. Tang et al and Kang et al. [1, 8] found two reduction peaks for CoO_x/CeO_2 catalyst, which were attributed to the step-wise reduction of cobalt oxide via $Co^{3+} \rightarrow Co^{2+} \rightarrow Co^0$. According to the above reports, we suggest the peak α_1' at 322 °C is attributed to the reduction of Co^{3+} to Co^{2+}, the peak β_1' at 356 °C and the shoulder one at 400 °C are ascribed to the reduction of Co^{2+} to Co^0. The reduction profile of $Cu_{0.4}Co_{0.6}Ce_4$ catalyst is characterized by the reduction peaks at about 168, 197, 265, 308 and 398 °C, labeled as α_2, β_2, α_2', β_2' and γ_2'.The peaks at 168, 197 °C are due to the reduction of CuO strongly interacting with CeO_2 and the larger CuO particles less combined with CeO_2, respectively. Additionally, the peak at 265 °C corresponds to the reduction of Co^{3+} to Co^{2+}, and the peaks at 308 and 398 °C are assigned to the reduction of Co^{2+} to Co^0.

It is of interest to find out that the reduction peaks of CuO in $Cu_{0.4}Co_{0.6}Ce_4$ shift toward lower temperature compared with that of Cu_1Ce_4. Although the CuO content in $Cu_{0.4}Co_{0.6}Ce_4$ is lower than that in Cu_1Ce_4, the intensity of peak α_2 increases markedly compared with peak α_1 observed in Cu_1Ce_4 catalyst. At the same time, the reduction peaks of Co_3O_4 in $Cu_{0.4}Co_{0.6}Ce_4$ also shift toward lower temperature compared with that of Co_1Ce_4. These results indicate that the addition of cobalt to the sample can improve the dispersion and enhance the reducibility of copper species, and the existence of the copper species can also favor the reducibility of the cobalt species. The synergetic interaction between copper and cobalt species would promote the reducibility of the catalyst. Simultaneously, the effect of the smaller nanoparticles may be also involved.

The XP spectra were performed in order to further illuminate the surface composition and the chemical state of the elements existed in $Cu_{0.4}Co_{0.6}Ce_4$ catalyst calcined at 550 °C. Figure 6 presents the spectra of Ce 3d, Cu 2p and Co 2p. The Ce 3d spectrum in Fig. 6a shows six peaks at about 882.6, 888.5, 898.2, 900.9, 907.8 and 916.7 eV. The principle peaks of Ce $3d_{5/2}$ and Ce $3d_{3/2}$ are located at about 882.6 and 900.9 eV, respectively. The peaks at about 888.5 and 898.2 eV are the satellites raising from Ce $3d_{5/2}$ ionization, while the peaks at about 907.8 and 916.7 eV are that of Ce $3d_{3/2}$ ionization. Nelson and Schulz [30] reported that the peaks at 903.2–903.5 eV and 884.7–885.0 eV represented the $3d^{10}4f^1$ initial electronic state corresponding to Ce^{3+}, while the peaks at 915.9–916.1 eV and 897.5–897.8 eV represented the $3d^{10}4f^0$ state of Ce^{4+} ions. Zhang et al. [31] showed that the characteristic peaks of Ce_2O_3 occurred at 885.3 and 903.4 eV. Natile et al. [22] and Cao et al. [32] also reported a small peak of Ce^{3+} appeared at about 885.6 eV. For this study, the peak corresponding to Ce^{3+} cannot be found in Fig. 6a, while the peak corresponding to Ce^{4+} ion can be found at about 898.2 and 916.7 eV. This indicates the main valence of cerium in the $Cu_{0.4}Co_{0.6}Ce_4$ catalyst is +4.

The Cu 2p XP spectrum in Fig. 6b shows two main peaks of Cu $2p_{3/2}$ and Cu $2p_{1/2}$ at about 934.2 and 954.1 eV. Additionally, there were satellite peaks in the range of 940.7–944.5 eV. It is reported that Cu^{2+} has satellite peaks while Cu^+ does not [33]. The presence of the main peak at about 934.2 eV and the shake-up peaks at about 940.7–944.5 eV indicates the existence of Cu^{2+} on the surface of the catalyst.

The peaks of Co 2p XP spectrum at 780.2 and 795.6 eV in Fig. 6c correspond to the peaks of Co $2p_{3/2}$ and Co $2p_{1/2}$, respectively. Vob et al. [29] reported that the XPS peaks of Co_3O_4 centered at 780.2 and 795.5 eV. Thus, we deduce

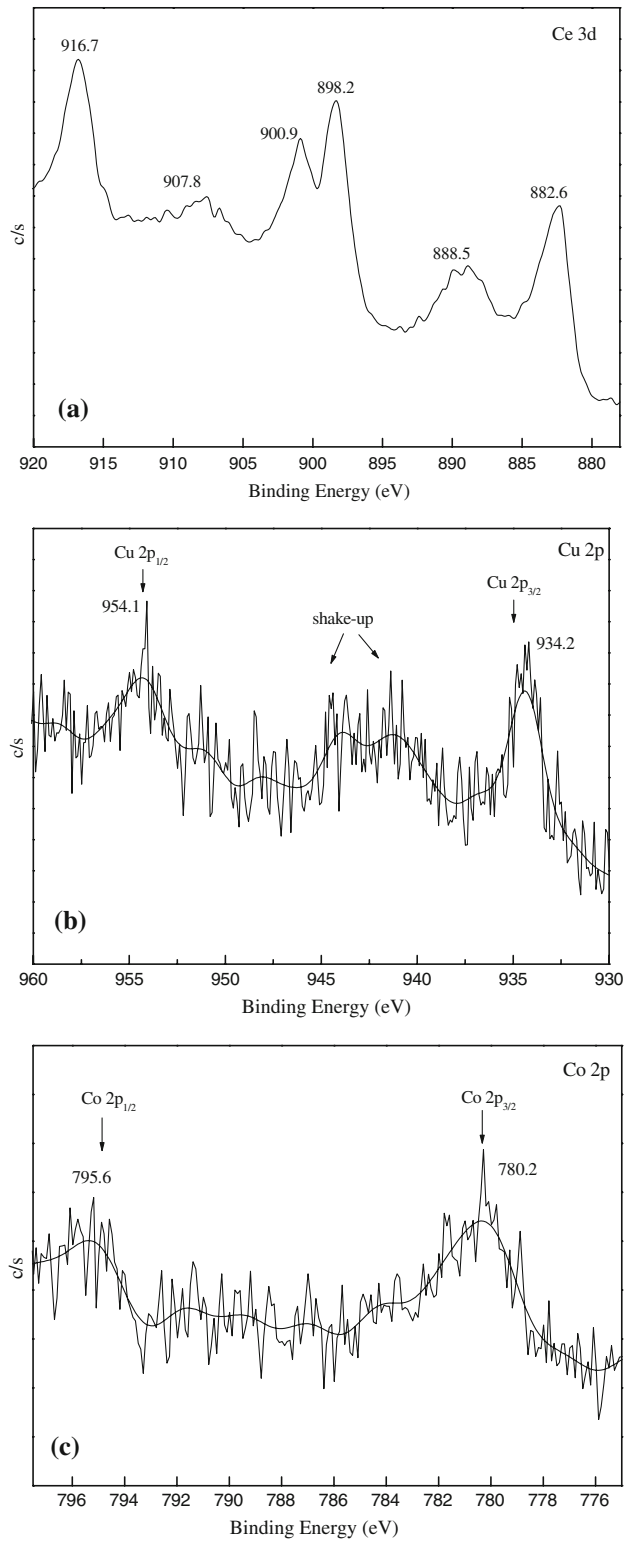

Fig. 6 XP spectra of $Cu_{0.4}Co_{0.6}Ce_4$ catalyst: (**a**) Ce 3d, (**b**) Cu 2p, (**c**) Co 2p

that the cobalt species in $Cu_{0.4}Co_{0.6}Ce_4$ catalyst exists as Co_3O_4, which is also consistent with the XRD and IR results.

The surface atomic ratio of Cu/(Cu + Co + Ce) obtained from XPS is 0.172, which is much higher than the nominal atomic ratio (0.064) obtained from ICP-AES. This result demonstrates that the copper oxide species are enriched considerably on the surface. The surface atomic ratio of Co/(Cu + Co + Ce) obtained from XPS is 0.091, which is approximately consistent with the nominal atomic ratio (0.078) obtained from ICP-AES.

3.2 Catalytic Performance for CO Oxidation

3.2.1 The Performances of the Cu–Ce–O Catalysts

In order to investigate the effect of CuO content on the performances of Cu–Ce–O catalysts prepared by co-precipitation, the activities of the Cu–Ce–O catalysts for low temperature CO oxidation were studied. Figure 7 shows the CO conversion over the Cu–Ce–O catalysts with different Cu/Ce atomic ratios calcined at 550 °C. The catalyst with the Cu/Ce atomic ratio of 1/4 is the most active for low temperature CO oxidation among the studied catalysts. It is reported that the finely dispersed CuO is responsible for the high catalytic activity for low-temperature CO oxidation, while the bulk CuO contributes little to the activity [13]. It is possible that the content of the well dispersed CuO in the $Cu_{0.7}Ce_4$ catalyst are smaller than that in the Cu_1Ce_4 catalyst. When the CuO content further increases, the bulk CuO increases, deteriorating the catalytic activity of the catalyst. Therefore, the Cu_1Ce_4 catalyst was selected for the following study.

3.2.2 The Performances of the Cu–Co–Ce–O Catalysts

The catalytic properties of the prepared Cu–Co–Ce–O catalysts with different Co/Cu atomic ratios for low

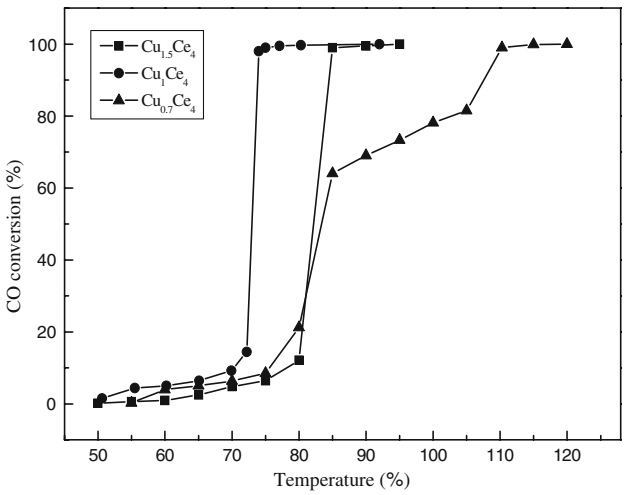

Fig. 7 Catalytic activities of Cu_xCe_4 catalysts with different copper oxide contents calcined at 550 °C

temperature CO oxidation were tested. The CO conversions of the Cu–Co–Ce–O catalysts as a function of reaction temperature are shown in Figs. 8 and 11. The "light-off" temperatures for 100% CO conversion ($T_{100\%}$) of the catalysts are shown in Table 1.

For comparison, the catalytic activities of CuO, CeO_2, Co_3O_4, Cu_1Ce_4 and Co_1Ce_4 catalysts are also included in Fig. 8. As can be seen that the catalytic activities of single CuO and CeO_2 oxides are much lower than those of Cu–Co–Ce–O catalysts. Co_3O_4 shows better catalytic performance than CuO and CeO_2, however, it is inferior to Cu–Co–Ce–O catalysts. The $T_{100\%}$ of the Cu–Co–Ce–O catalysts with Co/Cu atomic ratios of 1/1, 3/2 and 4/1 are lower than that of Cu_1Ce_4 catalyst, while the $T_{100\%}$ of the Cu–Co–Ce–O catalysts with Co/Cu atomic ratios of 1/4 and 2/3 and Co_1Ce_4 are higher than that of Cu_1Ce_4 catalyst. From Fig. 9, It can be found that the catalytic activities of the Cu–Co–Ce–O catalysts increase with the increase of Co content, and the catalyst with Co/(Cu + Co) atomic ratio of 0.6, corresponding to 3/2 in terms of Co/Cu atomic ratio, shows the best catalytic property. When the Co/(Cu + Co) atomic ratio is above 0.6, the activities of the catalysts decrease, suggesting that there must be a proper Co/Cu atomic ratio in the most active Cu–Co–Ce–O catalysts.

The calculations from Shapovalor [5] for the CeO_2 surface doped with Au, Ag, and Cu show that the bonds between the oxygen and the metal atoms is weakened by the presence of the dopant. In consideration of the IR results that Co–O bond in $Cu_{0.4}Co_{0.6}Ce_4$ is weaker than Co_1Ce_4 and the TPR results that the interaction between cobalt and copper can enhance the reducibility of each other, It seems that the synergetic interaction among the

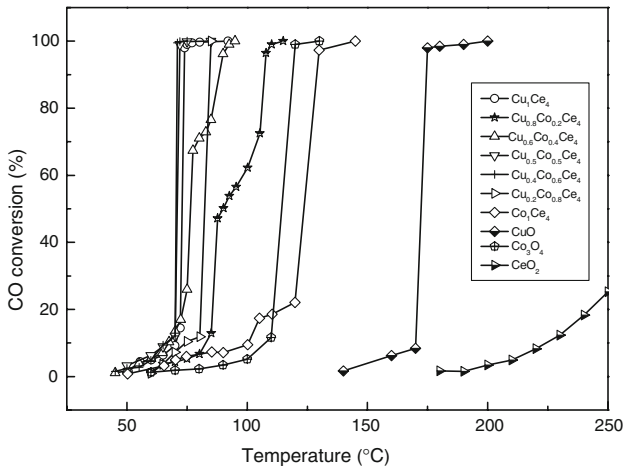

Fig. 8 Catalytic activities of Cu_1Ce_4, Co_1Ce_4, $Cu_xCo_{1-x}Ce_4$, CuO, Co_3O_4 and CeO_2 catalysts calcined at 550 °C

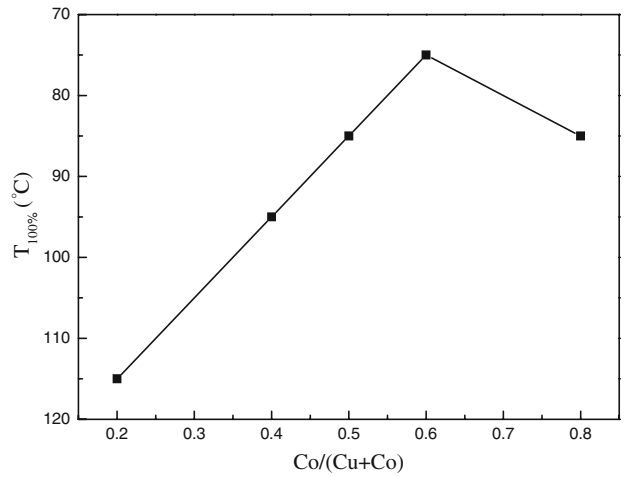

Fig. 9 Catalytic activities of $Cu_xCo_{1-x}Ce_4$ catalysts with different Co/(Cu + Co) atomic ratios calcined at 550 °C

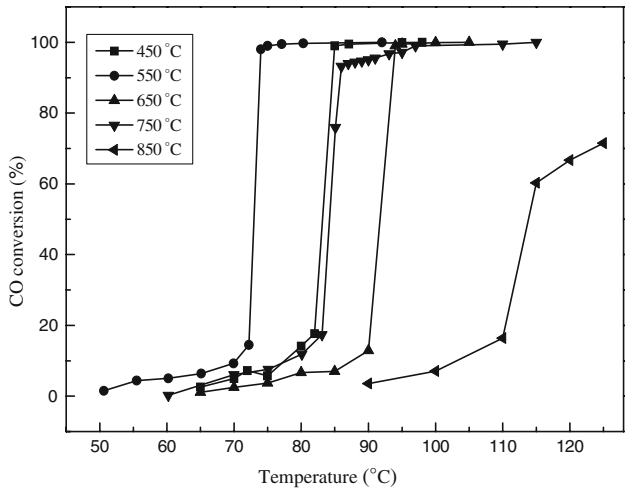

Fig. 10 Catalytic activities of Cu_1Ce_4 catalysts calcined at different temperatures

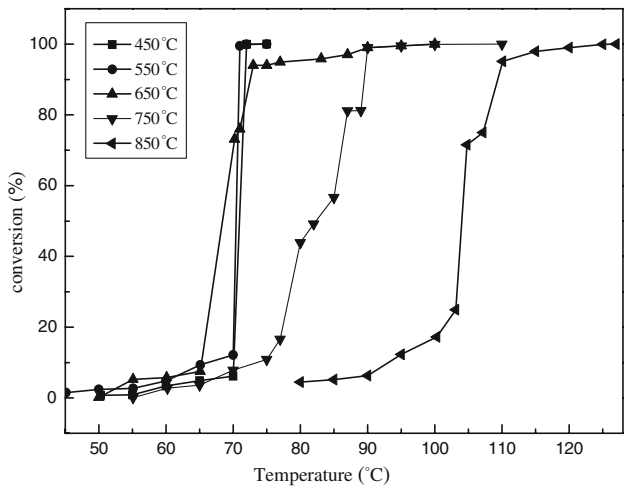

Fig. 11 Catalytic activities of $Cu_{0.4}Co_{0.6}Ce_4$ catalysts calcined at different temperatures

copper, cobalt, and ceria species would weaken the surface Cu–O bond and Co–O bond, and hence facilitating oxygen transfer and promoting the catalytic activity of the catalyst. When the Co/Cu atomic ratio is close to 3/2, the synergetic interaction is maximized.

Figures 10 and 11 show the catalytic activities of $Cu_{0.4}Co_{0.6}Ce_4$ and Cu_1Ce_4 catalysts calcined at different temperatures for low temperature CO oxidation. It can be seen that the catalytic activities of both catalysts decrease with the increase of calcinations temperature. When the calcination temperature increases to 850 °C, the catalytic activities decrease sharply. From XRD analysis, the decline of the catalytic activity with the increase of calcination temperature may be related to the growth of the catalyst and CuO particles. From Table 1, it also can be observed that the $T_{100\%}$ of $Cu_{0.4}Co_{0.6}Ce_4$ catalysts calcined at different temperatures are much lower than those of Cu_1Ce_4 catalysts, illuminating that the $Cu_{0.4}Co_{0.6}Ce_4$ catalysts have better activity than Cu_1Ce_4 catalysts. The $T_{100\%}$ of the $Cu_{0.4}Co_{0.6}Ce_4$ and Cu_1Ce_4 catalysts calcined at 850 °C are 127 and 180 °C, respectively, suggesting that the $Cu_{0.4}Co_{0.6}Ce_4$ should have better thermal resistance than the Cu_1Ce_4.

Based on the above, it can be seen that the $Cu_{0.4}Co_{0.6}Ce_4$ catalyst shows the best catalytic activity among all the prepared catalysts. The Co/Cu atomic ratio and the calcination temperature have obvious influence on the catalytic performances of the prepared Cu–Co–Ce–O catalysts for low temperature CO oxidation.

4 Conclusion

In the present study, the Cu–Ce–O and Cu–Co–Ce–O catalysts were prepared via a co-precipitation method. From XRD analysis, cubic, fluorite structure of CeO_2 is observed for all the Cu–Ce–O and Cu–Co–Ce–O catalysts. The XPS analysis show that the valence states of cerium and copper in $Cu_{0.4}Co_{0.6}Ce_4$ catalyst are +4 and +2, respectively, and cobalt exists as Co_3O_4. H_2-TPR results indicate that the addition of cobalt to Cu–Ce–O can improve the dispersion of copper species and enhance the reducibility of the catalyst, and the presence of the copper can also favor the reducibility of the cobalt species. The synergetic interaction among copper, cobalt and ceria species would promote the catalytic activity of the catalyst for CO oxidation. The catalytic activity studies demonstrate that the Co/Cu atomic ratio and the calcination temperature can affect the catalytic performances of the catalysts for CO oxidation. The $Cu_{0.4}Co_{0.6}Ce_4$ catalyst shows the best activity among all the prepared Cu–Co–Ce–O catalysts and has better activity and thermal resistance than Cu_1Ce_4 catalyst. This system is worthy investigating further.

Acknowledgments This work was supported by the National Nature Science Foundation of China (No. 20771061) and 973 program (2005CB623607).

References

1. Tang CW, Kuo CC, Kuo MC, Wang CB, Chien SH (2006) Appl Catal A 309:37
2. Zheng XC, Zhang XL, Wang XY, Wang SR, Wu SH (2005) Appl Catal A 295:142
3. Luo MF, Ma JM, Lu JQ, Song YP, Wang YJ (2007) J Catal 246:52
4. Tabakova T, Idakiev V, Papavasiliou J, Avgouropoulos G, Ioannides T (2007) Catal Commun 8:101–106
5. Shapovalov V, Metiu H (2007) J Catal 245:205
6. Sundar RS, Deevi S (2006) J Nanopart Res 8:497
7. Cao JL, Wang Y, Yu XL, Wang SR, Wu SH, Yuan ZY (2007) Appl Catal B 79:26
8. Kang M, Song MW, Lee CH (2003) Appl Catal A 251:143
9. Harrison PG, Ball IK, Azelee W, Daniell W, Goldfarb D (2000) Chem Mater 12:3715
10. Tada M, Bal R, Mu XD, Coquet R, Namba S, Iwasawa Y (2007) Chem Commun 4689
11. Zheng XC, Wang SP, Wang XY, Wang SR, Wang XY, Wu SH (2005) Matter Lett 59:2769
12. Zheng XC, Wu SH, Wang SP, Wang SR, Zhang SM, Huang WP (2005) Appl Catal A 283:217
13. Wang SP, Wang XY, Huang J, Zhang SM, Wang SR, Wu SH (2007) Catal Commun 8:231
14. Sirichalprasert K, Luengnaruemitchai A, Pongstabodee S (2007) Int J Hydrogen Energy 32:915
15. Chen YZ, Liaw BJ, Huang CW (2006) Appl Catal A 302:168
16. Jansson J, Palmqvist AEC, Fridell E, Skoglundh M, Österlund L, Thormählen P, Langer V (2002) J Catal 211:387
17. Thormählen P, Skoglundh M, Fridell E, Andersson B (1999) J Catal 188:300
18. Haneda M, Kintaichi Y, Bion N, Hamada H (2003) Appl Catal B 46:473
19. Mergeler YJ, van Aalst A, van Delft J, Nieuwenhuys BE (1996) Appl Catal B 10:245
20. Qian K, Huang WX, Jiang ZQ, Sun HX (2007) J Catal 248:137
21. Luo JY, Meng M, Qian Y, Zou ZQ, Xie YN, Hu TD, Liu T, Zhang J (2007) Catal Lett 116:50
22. Natile MM, Glisenti A (2005) Chem Mater 17:3403
23. Christoskova StG, Stoyanova M, Georgieva M, Mehandjiev D (1999) Mater Chem Phys 60:39
24. Singh RN, Pandey JP, Singh NK, Lal B, Chartier P, Koenig JF (2000) Electrochim Acta 45:1911
25. Tang CW, Yu WY, Wang CB, Chien SH (2007) Catal Lett 116:161
26. Yao HC, Yao YFY (1984) J Catal 86:254
27. Avgouropoulos G, Ioannides T (2003) Appl Catal A 244:155
28. Liu W, Flytzani-Stephanopoulos M (1996) Chem Eng J 64:283
29. Vob M, Borgmann D, Wedler G (2002) J Catal 212:10
30. Nelson AE, Schulz KH (2003) Appl Surf Sci 210:206
31. Zhang YW, Si R, Liao CS, Yan CH, Xiao CX, Kou Y (2003) J Phys Chem B 107:10159
32. Cao JL, Wang Y, Zhang TY, Wu SH, Yuan ZY (2007) Appl Catal B 78:120
33. Vepřek S, Cocke DL, Kehl S, Oswald HR (1986) J Catal 100:250